



Long-wave (10 μm) infrared light emitting diode device performance

Naresh C. Das^{a,*}, John Bradshaw^b, Fred Towner^b, R. Leavitt^b

^a Microphotonics Branch, Army Research Laboratory, 2800 Powder Mill Road, Adelphi, MD 20783, United States

^b Maxion Technologies Inc., 5000 College Avenue, Suite 3121, College Park, MD 20782, United States

ARTICLE INFO

Article history:

Received 15 April 2008

Received in revised form 9 September 2008

Accepted 11 September 2008

The review of this paper was arranged by Prof. A. Zaslavsky

Keywords:

LED device

Surface emitting devices

IR scene projection

LWIR emitters

ABSTRACT

Electroluminescence in the range of 6–12 μm is observed from an Sb-based type-II interband quantum cascade structure. The LED structure has 30 active/injection periods. We have studied both top-emitting and flip-chip mount bottom emitting LED devices. For room temperature operation, an increase, saturation and decrease in light output occur at successively higher injection currents. An increase of about 10 times in light output occurs when device is operated at 77 K compared to room temperature operation. This increase is attributed to reduced Auger non-radiative recombination at lower temperatures. The peak-emission wavelengths at room temperature and 80 K operation are 7 and 10 μm , respectively. These devices can be used for high-temperature simulation in an infrared scene generation experiment.

© 2008 Elsevier Ltd. All rights reserved.

1. Introduction

Efficient semiconductor light sources for the longer-wavelength (>6 μm) infrared (IR) spectral region are in growing demand for many military and commercial applications. For example, IR light emitting sources are the heart of the hardware-in-the-loop (HWIL) application. Also there exists a great demand for large-format two dimensional (2D) IR-emitter arrays with very good uniformity and reliable operation for IR scene projection experiments. Conventional low-band-gap semiconductor materials like lead salts [1,2] are currently employed for such applications. However, rather poor quality of these narrow-band-gap materials limits their performance. Few publications are available on long-wave IR (LWIR) light emitting diode (LED) devices [3]. Large-format (512 \times 512) silicon nitride resistor arrays have been used for IR scene projection experiments [4,5]. However, long-term reliability and maximum temperature of emission are still the largest issues for IR resistor technology for HWIL applications [6]. Digital micro mirror (DMD) arrays are also used to project IR scenes but with limited high-temperature and dynamic-range capabilities [7]. At Army Research Laboratory, we have developed an 8 \times 7 LWIR (10 μm) LED array for possible application in IR scene projection. In earlier papers [8,9], we have presented mid-wave IR LED results. The design, fabrication and testing of LWIR LED 2D arrays based on the inter-

band cascade (IC) LED structure and working with peak-emission at 10 μm are reported in this paper.

2. Experimental

The IC LED structure was grown by molecular beam epitaxy on an n-type 500 μm thick GaSb substrate. The active region, sandwiched between a 1.4 μm -thick top p-type contact layer and a 0.4 μm bottom contact layer, consists of 30 cascaded active/injection periods. The top contact layer of 1.4 μm is used for grating formation to improve the light output efficiency. Fig. 1 shows the band diagram of an InAs/GaInSb/AlSb type-II interband cascade device with one active region and one injection region. In our LED structure the active region contained an additional InAs quantum well (QW) inserted between the GaInSb and AlSb layers, forming asymmetric QWs similar to the W structure of reference [10]. Each period includes an asymmetric InAs/GaInSb/InAs “W” quantum well preceded by an n-type digitally-graded InAs/Al(In)Sb injector. The layer after GaSb layer in active region is AlSb layer. The n-type injection region serves as the collector and emitter for the preceding and following active regions, respectively. The whole multi-layer structure is strain-balanced and lattice-matched to the GaSb substrate. Under a forward bias, electrons are injected from an injection region into the level E_e which is in the band gap region of the adjacent GaInSb layer. Since the electrons at the level E_e are effectively blocked from directly tunneling out of the GaInSb and AlSb layers, they tend to relax to the hole state E_h in the adjacent

* Corresponding author.

E-mail address: ndas@arl.army.mil (N.C. Das).

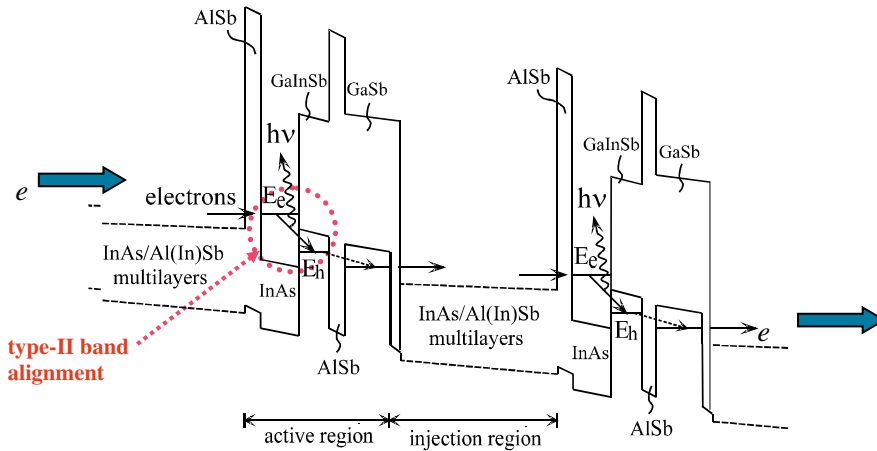


Fig. 1. Band diagram of type-II interband cascade structure.

valence band quantum well, resulting in photon emission. Electrons at state E_h can then cross the thin AISb barrier and GaSb layer by tunneling into the conduction band of the next injection region because of strong spatial interband coupling and are ready for the next interband transition resulting in photon emission.

The LED fabrication process starts with reactive ion etching of the mesa area down to the bottom contact layer. The total etch depth is about $3.0\ \mu\text{m}$. The square mesa size of each pixel in the 8×7 array is $100\ \mu\text{m}$ on a side unless otherwise indicated. For comparison, we have also tested LED devices with a square mesa varying between 30 and $200\ \mu\text{m}$ on a side. Silicon nitride is deposited by the PECVD technique, after which contact windows are opened and a Ti/Au metal layer is deposited. After the LED array fabrication on the GaSb substrate, the array is flip-chip mounted onto a silicon fan-out array. Lastly the bottom GaSb substrate is thinned by lapping and polishing leaving only $50\ \mu\text{m}$ of GaSb substrate material. Light is observed from the substrate side on all flip-chip mounted arrays. We have also studied LED devices with top emission without flip-chip bonding. In those cases, we used a different set of masks with a top metal opening for light to pass through.

3. Results and discussion

The light was collected and collimated by a lens with 2-in.-aperture and 2 in.-focal length. The HgCdTe detector was placed at the focus of a second 1-in.-focal length lens. We used pulsed injection current of different pulse widths and duty cycles for light emission measurements. We observed maximum light output for injection current of pulse width $6\ \mu\text{s}$ and 30% duty cycle. Hence these parameters were fixed at those values for subsequent measurements with different injection currents. In Fig. 2, we present the room temperature light emission power versus LED injection current density for different mesa sizes. The total output power increases monotonically but not linearly with LED mesa size. For example with 100-mA/area pulsed injection current density, 50- μm -square LED has light output power of about $0.75\ \mu\text{W}$ whereas for a 100- μm -square device (four times the area) the power is about $2.21\ \mu\text{W}$. From the I curves we observed optical output saturation as well as ultimately a decrease of optical output at progressively higher injection currents.

Larger device attain saturation and decrease of light out put power at lower current density than smaller device. This can be attributed to more thermal leakage current and other possible enhanced non-radiative carrier recombination processes at higher junction temperatures [11].

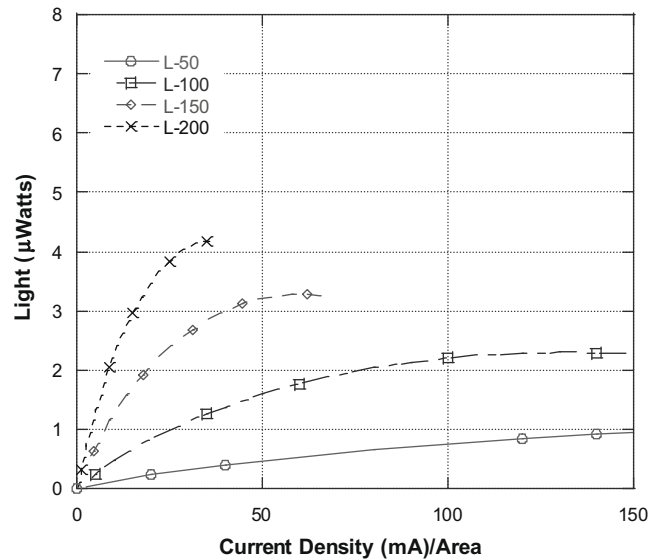


Fig. 2. Light output from the flip-chip devices versus injection pulsed current density for square mesa sizes of 50, 100, 150 and $200\ \mu\text{m}$ on a side.

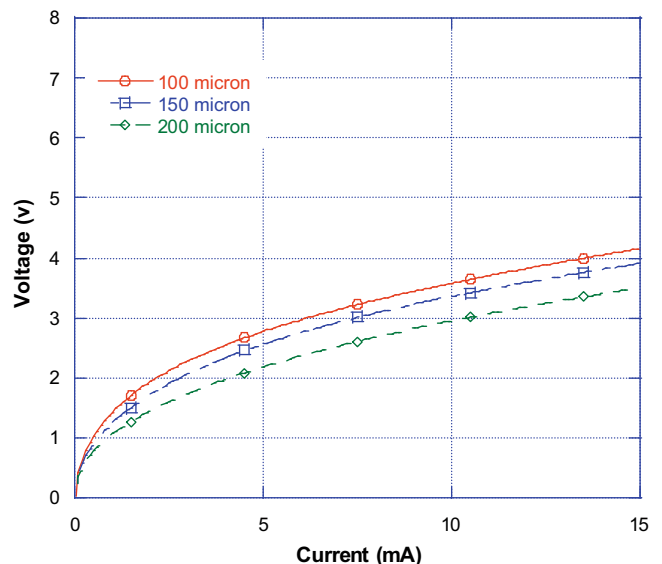


Fig. 3. Current and voltage curves for three mesa size devices.

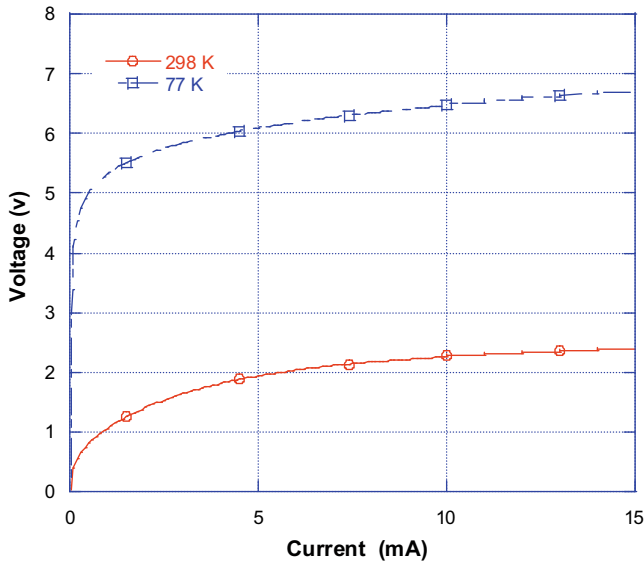


Fig. 4. *IV* characteristics at room temperature and 77 K for 100- μm top-emitting LED.

The current–voltage (*IV*) curves for different DC injection currents are shown in Fig. 3. The 200- μm device has the least voltage drop among the three devices shown here, which is not surprising since it has the least resistance. However, for all the devices we observed a similar rate of increase of voltage with increasing injection current.

Typical current–voltage (*IV*) curves of a 100- μm device taken at temperatures of 77 K and 298 K are shown in Fig. 4. This is the top-emitting device with epi up configuration. It is not flip-chip mounted, in contrast to the devices reported in Figs. 2 and 3. The turn-on voltage increases by a factor of 3 when decreasing the device operating temperature from 298 to 77 K, indicating the reduction of some parasitic processes with decreasing temperature. We also measured a large increase (10 times) of light output at 77 K compared to room temperature LED emission power (as shown in Fig. 5) as the LED becomes a progressively more idealized type-II super lattice emitter. The large increase of light output at 77 K compared to room temperature is mostly due to reduced Au-

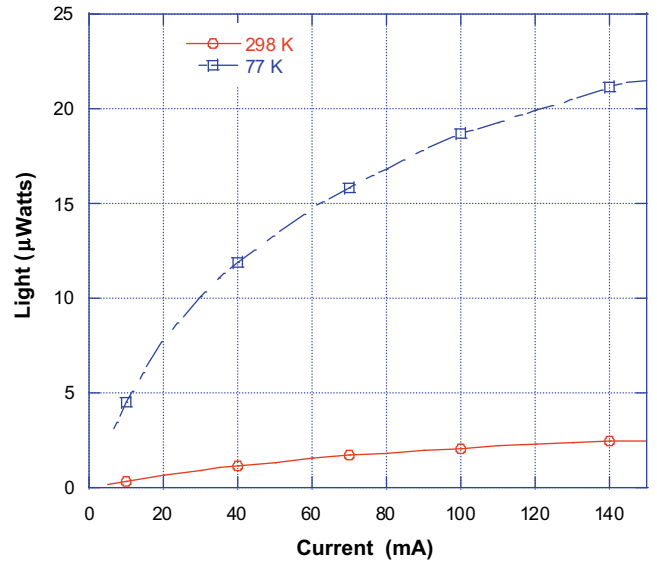


Fig. 5. *LI* characteristics at room temperature and 77 K for 100- μm top-emitting LED.

ger recombination at lower temperature, which is the dominant source of non-radiative recombination processes and exponentially increases with temperature [12].

As shown in Fig. 6a, the electroluminescence from a flip-chip LED at room temperature has its spectral peak at about 10 μm . Very little shift in peak-emission wavelength occurs by changing the injection current from 20 to 40 mA. Fig. 6b shows the top-emitting LED spectra at 80 K. The peak-emission (from same material) shifts to 7 μm due to temperature reduction. Again we did not observe any appreciable shift in peak-emission wavelengths for two injection current values. At room temperature the spectrum becomes broader and shifts to longer-wavelength due to decrease of the band gaps.

The light emission from MBE grown IC LED structure was observed for different mesa size devices at various temperatures. The light output characteristics from LWIR LED devices depend on many factors such as design and growth parameters, processing techniques, device temperature, carrier relaxation and radiative

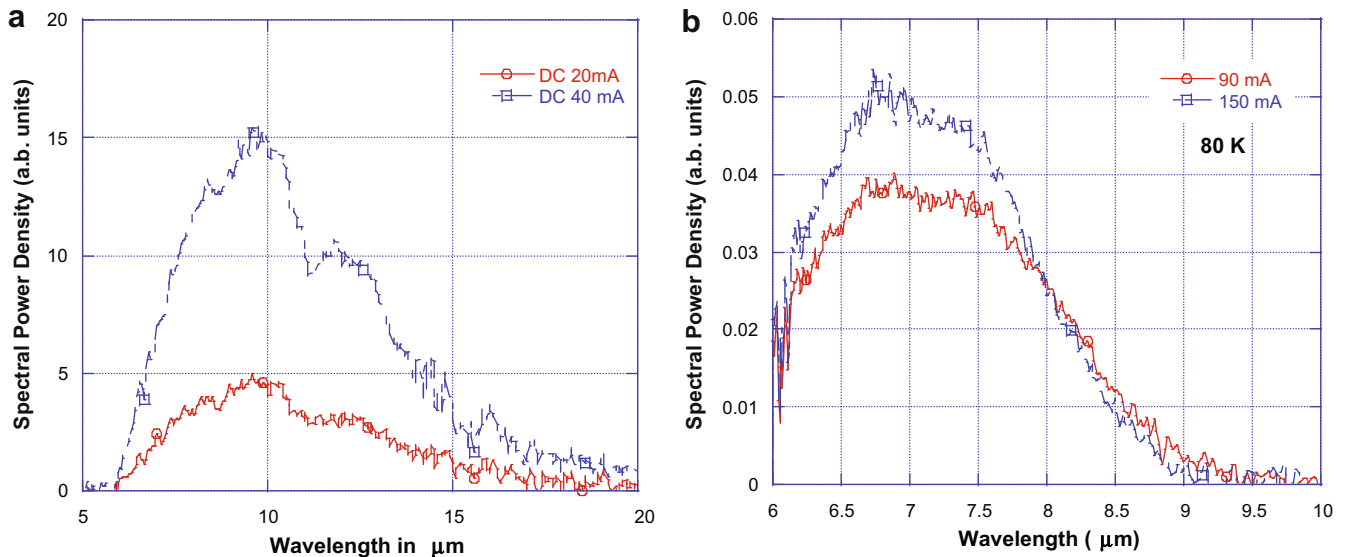


Fig. 6. (a) Room-temperature flip-chip 100- μm LED spectra and (b) 80 K top-emitting 100- μm LED spectra.

recombination [13] phenomena. The details of the observed electroluminescence power depend upon balance of these processes. At room temperature and low injection current density values (Fig. 2), the increase in output power is due to carrier injection and recombination at trap sites [14]. The injection current values corresponding to peak power at different temperatures are the characteristic value of the QW structure and device size. For higher injection current above the peak-emission value, various non-radiative processes like phonon relaxation become dominant [15] and hence light output power decreases. However, for top-emitting devices (Fig. 5) we did not observe any decrease in light emission at higher injection currents. For bottom emitting devices, with increase of injection currents the voltage compliance also increases as seen in Fig. 3. It is due to various non-radiative recombination processes occur at higher injection currents. The large increase in optical power at cryogenic temperature (Fig. 5) may be due to reduction in Auger recombination process at lower temperatures [16,17]. By comparing Figs. 2 and 5, we observed less saturation characteristics of light output power for top-emitting devices compared to flip-chip mount devices. This may be due to better cooling in top-emitting devices as the GaSb substrate is mounted directly on the cryostat, whereas heat conduction for flip-chip mount devices is through silicon fan-out chip. We measured optical power up to 22 μW much higher than the maximum power reported for intersubband QC LEDs [18]. This indicates an improved radiative and collection efficiency.

In summary, we have demonstrated electroluminescence in the 6–12 μm spectral range from Sb-based interband cascade LED devices fabricated in top-emitting and flip-chip configurations. We have studied devices with various mesa sizes and operating at both room and cryogenic temperatures. The optical power is the highest reported so far from interband cascade structure LWIR LED devices. These devices can be used for IR scene generation experiments as thermal sources to simulate high-temperature targets as well as for many other sensor applications.

Acknowledgement

The authors would like to thank Dr. David M. Mackie for technical discussion.

References

- [1] Shi Z, Tacke M, Lambrecht A, Bottner H. Mid-infrared lead salt multi quantum well diode lasers with 282 K operation. *Appl Phys Lett* 1995;66:2537.
- [2] Brett Beasley D, Saylor DA, Bufford J. Overview of dynamic scene projectors at the U.S. Army aviation and missile command. *Proc SPIE* 2002;4717:136.
- [3] Zhang D, DuPont E, Yang RQ, Liu HC, Lin H, Buchanan M, et al. Long wave length infrared (10–12 μm) electroluminescence from Sb based interband cascade device. *Opt Exp* 1991;1:97.
- [4] Cole B et al. Large area infrared micro emitter arrays for dynamic scene projection. *Proc SPIE* 1998;3368:57.
- [5] McHugh S, Robinson R, Parish B, Woolaway J. *Proc SPIE* 2000;4027:399.
- [6] Driggers R, Barnard K, Burroughs E, Deep RG, Williams O. Review of infrared scene projector technology. *Opt Eng* 1994;33:2408.
- [7] Das NC. Increase in mid-wave infrared light emitting diode light output due to substrate thinning and texturing. *Appl Phys Lett* 2007;90:111111.
- [8] Beasley DB et al. Dynamic IR scene projector based upon the digital micromirror device. *Proc SPIE* 2001;4366:96.
- [9] Das NC, Tobin MS. Performance of mid-wave infrared (3.8 μm) light emitting diode device. *Solid State Electron* 2006;50:1612.
- [10] Meyer JR, Hoffman CA, Bartoli FJ, Ram Mohan LR. Type II quantum well lasers for the mid infrared. *Appl Phys Lett* 1995;7:757.
- [11] Yang RQ, Lin C, Murry SJ, Pei SS. Interband cascade light emitting diodes in the 5–8 μm spectrum region. *Appl Phys Lett* 1997;70:2013.
- [12] Zegrya GG, Andreev AD. Mechanism of suppression of Auger recombination processes in type-II heterostructures. *Appl Phys Lett* 1995;67:2681.
- [13] Pidgeon CR, Ciesla CM, Murdin BN. Suppression of non-radiative processes in semiconductor mid-infrared emitters and detectors. *Prog Quant Electron* 1998;21:361.
- [14] Stringfellow GB, Craford MG. High brightness light emitting diode. *Semiconductors and semimetals*, vol. 48; 1997. p. 469.
- [15] Krier A, Gao HH, Sherstnev VV, Yakovlev Y. *J Appl Phys* 1999;D 32:3117.
- [16] Horikoshi Y. In: Tsang WT, editor. *Semiconductors and semimetals*, vol. 22C. New York: Academic; 1985 [chapter 3].
- [17] Smith DL, Mailhoit CM. *J Appl Phys* 1987;62:2545.
- [18] Faist J, Capasso F, Sirtori C, Sivco DL, Hutchinson AL, Chu SN, et al. *Appl Phys Lett* 1994;64:1144.